International Society for Biofabrication
PURPOSE-LED PUBLISHING™

PAPER • **OPEN ACCESS**

Cancer-mediated axonal guidance of sensory neurons in a microelectrode-based innervation MPS

To cite this article: Matthijs van der Moolen *et al* 2024 *Biofabrication* **16** 025013

View the article online for updates and enhancements.

You may also like

- Imaging three-dimensional innervation zone distribution in muscles from M-wave recordings
Chuan Zhang, Yun Peng, Yang Liu et al.
- Self-assembled innervated vasculature-on-a-chip to study nociception
Vardhman Kumar, David Kingsley, Sajeeshkumar Madhurakkat Perikamana et al.
- Activation thresholds for electrical phrenic nerve stimulation at the neck: evaluation of stimulation pulse parameters in a simulation study
Laureen Wegert, Marek Ziolkowski, Tim Kalla et al.

GAS

BreathSpec®

The combination of GC and IMS enables a physical separation to detect volatiles without pre-concentration directly sampled from human breath.

Our GC-IMS based analyzer allows instant breath sampling and analysis of volatiles in minutes.

The transportable GC-IMS facilitates versatile sampling incl. direct exhalation, syringe based and also gas bags for sampling of breath and static body headspace (oral/nasal/skin).

▶▶▶ click for more details

This content was downloaded from IP address 80.254.185.209 on 10/04/2026 at 14:27

Biofabrication

PAPER

Cancer-mediated axonal guidance of sensory neurons in a microelectrode-based innervation MPS

Matthijs van der Moolen[1,2], **Andrea Lovera**[3], **Fulya Ersoy**[1,2], **Sacha Mommo**[3], **Peter Loskill**[1,2] **and Paolo Cesare**[1,2,4,*]

[1] NMI Natural and Medical Sciences Institute at the University of Tübingen, Markwiesenstr. 55, 72770 Reutlingen, Germany
[2] Department for Microphysiological Systems, Institute of Biomedical Engineering, Eberhard Karls University Tübingen, Österbergstr. 3, 72074 Tübingen, Germany
[3] FEMTOprint SA, Via Industria 3, 6933 Muzzano, Switzerland
[4] Current address: Eurac Research, Institute for Biomedicine, via Volta 13A, 39100 Bolzano, Italy.
[*] Author to whom any correspondence should be addressed.

E-mail: paolo.cesare@nmi.de and paolo.cesare@eurac.edu

Keywords: microphysiological system, microelectrode array, dorsal root ganglia, pain, cancer

Supplementary material for this article is available online

OPEN ACCESS

RECEIVED
23 October 2023

REVISED
23 December 2023

ACCEPTED FOR PUBLICATION
23 January 2024

PUBLISHED
9 February 2024

Original content from this work may be used under the terms of the Creative Commons Attribution 4.0 licence.

Any further distribution of this work must maintain attribution to the author(s) and the title of the work, journal citation and DOI.

Abstract

Despite recent advances in the field of microphysiological systems (MPSs), availability of models capable of mimicking the interactions between the nervous system and innervated tissues is still limited. This represents a significant challenge in identifying the underlying processes of various pathological conditions, including neuropathic, cardiovascular and metabolic disorders. In this novel study, we introduce a compartmentalized three-dimensional (3D) coculture system that enables physiologically relevant tissue innervation while recording neuronal excitability. By integrating custom microelectrode arrays into tailored glass chips microfabricated via selective laser-etching, we developed an entirely novel class of innervation MPSs (INV-MPS). This INV-MPS allows for manipulation, visualization, and electrophysiological analysis of individual axons innervating complex 3D tissues. Here, we focused on sensory innervation of 3D tumor tissue as a model case study since cancer-induced pain represents a major unmet medical need. The system was compared with existing nociception models and successfully replicated axonal chemoattraction mediated by nerve growth factor (NGF). Remarkably, in the absence of NGF, 3D cancer spheroids cocultured in the adjacent compartment induced sensory neurons to consistently cross the separating barrier and establish fine innervation. Moreover, we observed that crossing sensory fibers could be chemically excited by distal application of known pain-inducing agonists only when cocultured with cancer cells. To our knowledge, this is the first system showcasing morphological and electrophysiological analysis of 3D-innervated tumor tissue *in vitro*, paving the way for a plethora of studies into innervation-related diseases and improving our understanding of underlying pathophysiology.

1. Introduction

Microphysiological systems (MPSs) technology has made significant strides in enabling the investigation of complex biological interactions in accurately represented organs and tissues. However, the importance of innervation for proper tissue function has been largely overlooked [1]. Peripheral innervation plays an essential role in mediating the response of skin, bone, muscles and visceral organs to environmental changes and maintaining tissue homeostasis [2–4]. Additionally, in diseases such as cancer, aberrant innervation patterns can have significant effects on pain, highlighting the critical role of innervation in pathological conditions. Therefore, incorporating nerves in three-dimensional (3D) *in vitro* models is urgently required. Although previous approaches have used micropatterned structures to manipulate axons by injury and/or growth factor cocktails, these are limited to two-dimensional (2D) space and not appropriate for innervation of complex 3D structures such as organoids and spheroids [5–9]. To

© 2024 The Author(s). Published by IOP Publishing Ltd

address these shortcomings, we developed a compartmentalized 9-well INV-MPS for coculture of peripheral nervous system (PNS) neurons with 3D tissues, all embedded in hydrogels. In addition, we have integrated microelectrode arrays (MEA) to allow direct and parallel recording of electrophysiological activity in 3D neurons with high spatio-temporal resolution, which is highly relevant to the study of sensory function, more physiological than calcium imaging and more efficient than patch-clamp recording [10]. This represents a substantial innovation over currently available MEA-based microfluidics, which are limited to 2D applications. Various MEA configurations have been commonly combined with poly-dimethylsiloxane (PDMS)-based microfluidics to study, for example, the sensitizing (painful) effects of exposing the PNS to the secretome of mature osteoclasts in bone disease [11]. Researchers also exploited MEA technology to create flexible polyimide-based devices that interface with unmyelinated C-fibers using protruding 3D gold pillars to record elusive low-amplitude neural signals in the nerve plexus [12]. Lastly, relevant work includes combining stereolithographic printing of polycarbonate devices and membranes with PDMS for placement inside multiwell MEA plates for functional analysis of iPSC-derived sensory neurons innervating spinal cord organoids [13] and skin [14]. As a proof-of-concept for the potential use of the newly developed INV-MPS for innervation studies, we specifically investigate sensory innervation of cancer spheroids. This is also motivated by the significant unmet medical needs associated with cancer-induced pain (CIP), as well as the extensive amount of literature available on nociceptive fibers, both *in vivo* and *in vitro,* and growing ethical concerns regarding *in vivo* animal research in this field.

The INV-MPS is fabricated by bonding a selectively laser-etched glass chip to a custom MEA, creating two individual compartments connected by micro-tunnels.Suspended in hydrogel, murine dorsal root ganglion (DRG) neurons and colorectal or pancreatic cancer cells are deposited into the respective compartments. Once axons extend through the barrier, interaction of neurites and cancer spheroids can be monitored via time-resolved live imaging and electrophysiological recording. Current literature, mainly based on *in vivo* studies, reveals an increase in nerve density/nerve alteration and pain states, also triggered by tumor-mediated release of factors such as NGF and prostaglandins (PGE_2) [15–21]. By exposing compartmentalized nerve terminals to pain and inflammatory mediators after applying a NGF gradient we confirmed the potent effect of NGF on inducing a nociceptive phenotype. Remarkably, in the absence of NGF, colorectal cancer spheroids were also able to attract sensory neurites and become innervated, accompanied by the induction of excitability through application of pain agonists. These findings suggest that cancer cells alone can drive a nociceptive phenotype, similar to NGF. Finally, live-imaging of Ca^{2+} transients in cancer-innervating fibers confirmed that the neurites are responsive to noxious stimuli while interacting closely with cancer cells. Functional innervation of cancer spheroids by sensory fibers as shown here serves as a case study for the INV-MPS, an innovative 3D *in vitro* model amenable for exploring tissue-induced axonal growth, nerve sprouting and associated changes in neuronal electrophysiology. However, the platform has the potential to benefit a much broader community of microphysiological scientists who aim to recapitulate and explore the complexity of innervated tissues. Thus, the INV-MPS represents a significant advancement towards novel human-relevant drug discovery models, particularly in pathologies where tissue innervation plays a critical role.

2. Results

2.1. A novel MPS with integrated electrodes for 3D axon manipulation and recording from sensory neuron cultures

Although MPSs have advanced with rapid strides recently, the development of new *in vitro* PNS models has been hampered by challenges in integrating effective readouts into complex 3D cultures. However, improving existing models, particularly with respect to tissue innervation, is critical for studying pathophysiological processes and the development of new therapeutic strategies. Therefore, we developed a novel MPS that integrates a non-invasive electrophysiological readout with glass microfluidics to produce a valuable 3D neurite outgrowth model that separates soma and axons. Specifically, we grew peripheral neurons in a 3D scaffold and facilitated their projection through a physical barrier, enabling them to innervate axonally residing tissue (figure 1(A) and movie S1). To achieve this, we produced a fused silica MPS patterned with μm-scale features and attached it to a MEA substrate, as previously described [10]. The MPS includes pairs of adjacent two-layer tissue wells (somatic and axonal compartment) featuring defined hydrogel layers (GL; approx. 8.0 μl) below media layers (ML; approx. 110.0 μl).

The two adjacent tissue wells are separated by a 300.0 μm thin barrier featuring 12 rows of 110 microtunnels (10.0 $\times$ 10.0 μm cross-section) each, over a surface area of approx. 4.0 $\times$ 1.0 mm (figure 1(B) and SI appendix, figure S1(A)). This 3D-arrangement of μ-tunnels is possible due to the unique capabilities of selective laser etching (SLE) that enables the selective removal of glass from a monolithic piece in 3D. The microtunnels (figure 1(C)) allow only DRG neurites to pass into the GL of the axonal compartment and constrain DRG cell bodies to the somatic compartment. To record

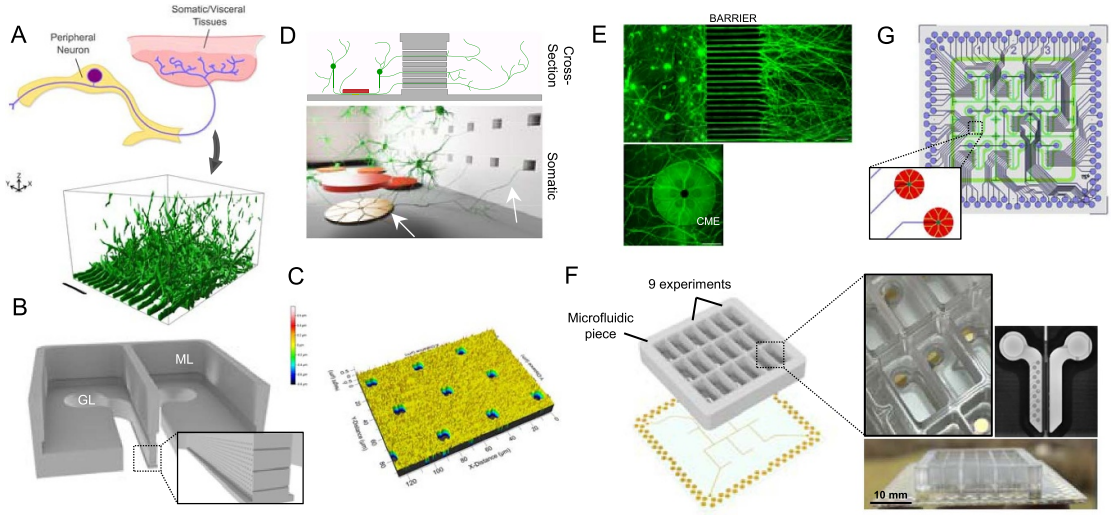

Figure 1. A novel MPS with integrated electrodes for 3D axon manipulation and recording from sensory neuron cultures. (A) Recapitulating the innervation of soft tissues by the peripheral nervous system. 3D-surface rendering of DRG terminals extending into 3D space in the axonal compartment. Dimensions 600 × 450 × 300 μm. (Scale bar: 100 μm). (B) Both somatic and axonal compartments are filled with a soft 3D scaffold inside the gel layer (GL). Supporting media is added on top in both media layers (ML) (width: 300.0 μm). (C) High magnification color map of micro tunneled barrier profilometry data. (D) DRG neurons grow neurites in 3D through the barrier while simultaneously projecting neurites into recording CMEs residing in the somatic compartment. (E) Live-cell confocal images (max projection) of GFP-transduced DRG homogeneously distributed across the somatic compartment with neurites traversing the barrier and entering CMEs (scale bar: 75 μm). (F) INV-MPS holds 9 identical cocultures with 13 CMEs each and assembles by bonding on top of the dedicated 120-electrode MEA. (G) Technical drawings of MEA-CME production photomasks.

from gel-embedded 3D neurons inside the INV-MPS, we utilized capped microelectrodes (CMEs) positioned at the base of the somatic compartment that effectively trap axons (figure 1(D)). Neurons occupying CME-microtunnels also extended towards the barrier and crossed into the axonal compartment in 3D. To confirm the spatial separation of soma and nerve terminals, we used live-cell confocal fluorescence microscopy of DRG neurons transduced with adenoviral vectors encoding enhanced green fluorescent protein (eGFP) (figure 1(E) and movies S2 and S3). Additionally, we confirmed that neurites grew inside the confined spaces of the CMEs (5.0 × 3.0 μm), allowing us to detect electrophysiological signals (up to ∼100 μV) generated upon firing of action potentials (SI appendix, figure S1(B)). Each micropatterned glass chip was bonded onto a 49.0 × 49.0 mm glass substrate containing 117 embedded recording electrodes. Thirteen recording-CMEs and a reference electrode were positioned within each of the nine somatic compartments. CMEs were connected to edge-pads, which secured the connection to pins of the MEA-recording system (figures 1(F) and (G)).

2.2. 3D axonal guidance and nerve terminal excitability modulated by NGF inside the MPS

Our study examined the responsiveness of 3D gel-embedded DRG neurons to neurotrophic gradients, which may have implications for tissue innervation under various pathophysiological conditions *in vivo*. We focused on NGF, a well-known neurotrophic factor that promotes the development of neuronal growth cones and can enhance neuronal survival *in vitro* [22, 23]. Here, experiments were performed using an INV-MPS without integrated electrodes (SLE INV-MPS; SI appendix, figure S2(C)), which features a single row of tunnels at the bottom of the barrier, allowing for accurate comparison of neurite outgrowth and microtunnel diffusion kinetics. To analyze the impact of NGF on 3D sensory fiber extension into the axonal compartment, we supplemented NGF solely axonally (NGF −/+), thereby creating a stable gradient over the barrier for 1 week. We found a significant increase in fibers crossing the barrier (figures 2(A) and (B) and SI appendix, figure S2(A)) with limited variability in survival across different conditions (SI appendix, figure S2(B)). When NGF was supplied to both compartments (NGF +/+), few axons extended through the barrier and neurites predominantly grew within the somatic compartment, likely due to the lack of a chemoattracting gradient. To mimic a NGF gradient across adjacent wells, we monitored the concentration of fluorescently labelled dextran moieties (applied to the axonal compartment) for 12 h and observed a ∼10*x* lower concentration of both 4 kDa and 20 kDa tracers in the somatic compartment. It is important to note that the small amount of dye that diffuses through the barrier is progressively diluted into a much larger volume in the somatic compartment, resulting in a significantly lower bulk concentration. Having

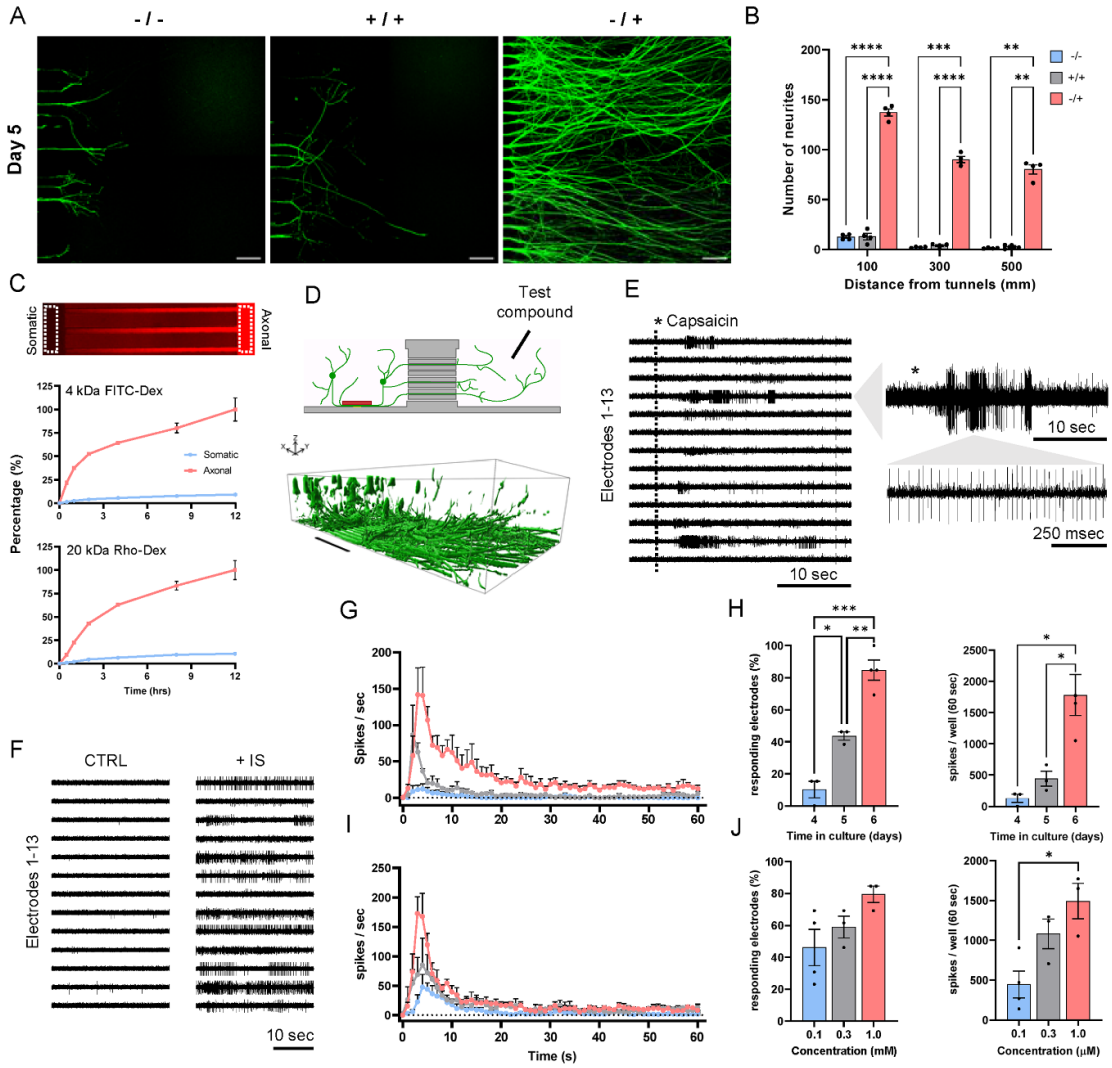

Figure 2. 3D axonal guidance and nerve terminal excitability modulated by NGF inside the MPS. (A) Live-cell confocal images of GFP-transduced DRG neurons protruding from the barrier in 3D after 5 d in culture. Neurobasal-A culture medium either contains no NGF (−/−), NGF in both somatic and axonal media compartment (+/+) or NGF only in the axonal media compartment (−/+) (scale bar: 75 μm). (B) Quantification of neurite outgrowth after 5 d in culture. Total number of neurites was measured at 100 μm, 300 μm, and 500 μm from the barrier. Bar graphs represent mean ± SEM ($n = 4$ wells) (C) micrograph shows diffusion of Dextran-FITC (MW: 4 kDa) or Dextran–Rhodamine B (MW: 20 kDa) through the micro-tunnel barrier from axonal (right) to somatic (left). Fluorescent intensity profiles generated from ROIs taken 5 μm from the micro-tunnel barrier, plotted against time as percentages (normalized to intensity at $T = 12$ h). Data is represented as mean ± SEM ($n = 3$ wells). (D) Agonists are applied to the media layer atop the 3D nerve terminals of a NGF −/+ culture in the axonal compartment. 3D-surface rendering of DRG neurons and their soma. Dimensions 1450 × 750 × 300 μm. (Scale bar: 300 μm). (E) Trace plots representing the activity recorded by 13 CMEs after application of 1 μM Capsaicin (black asterisk) at different time scales. (F) Trace plots comparing control to activity recorded 5 min after application of inflammatory soup (IS containing: 3.0 μM Bradykinin, 3.0. μM Prostaglandin, 3.0. μM Serotonin and 3.0 μM Histamine). (G) Temporal dynamics of Capsaicin (1 μM) responses in − rcultures of DRG neurons after 4 (blue), 5 (grey) and 6 (red) days. Dots represent the mean spikes per second per well over a 60-second span post-application ($n = 3$–4 wells). (H) Bar graphs comparing the development of nociceptive phenotype (percentage of responding electrodes) and total spikes recorded per well in the 60-second span post application at different time points (time in culture). (I) Dose-response plots comparing temporal dynamics following application of 0.1 (blue), 0.3 (grey) and 1.0 (red) μM capsaicin in −/+ cultures of DRG neurons ($n = 3$–4 wells). (J) Bar graphs comparing CMEs excitability probability (percentage of responding electrodes) and total spikes recorded per well in the 60-second span post application following application of different capsaicin's concentrations. In B, H, and J, significant differences between mean values of groups are displayed as asterisks: $*p < 0.05$; $**p < 0.01$; $***p < 0.001$; $****p < 0.0001$; Brown–Forsythe and Welch's ANOVA test.

optimized the conditions for neurite outgrowth in the SLE INV-MPS, we then transitioned to using the INV-MPS with integrated MEA for electrophysiological characterization of 3D sensory terminals in the NGF −/+ condition (figure 2(D)). Application of TRPV-1 agonist capsaicin [24] to the axonal compartment of the INV-MPS resulted in measurable action potentials in the majority of CMEs located in the somatic compartment (figure 2(E)). This provides evidence that compartmentalized 3D neuronal culture in the INV-MPS can successfully replicate peripheral activation of both receptors and ion channels involved in generating and transmitting nociceptive signals from nerve terminals to the soma. Recorded signals appeared within a timeframe of 3–5 s from administration of capsaicin, indicating the system's

ability to rapidly detect and measure terminally-evoked changes in neuronal activity. Given the non-invasive nature of MEA electrophysiological recordings, our system enables investigation into the long-term effects of substances within an inflammatory milieu. This was demonstrated by recording changes in neuronal activity induced by an inflammatory mediator cocktail (bradykinin, prostaglandin, serotonin and histamine), where action potentials could be continuously measured for up to 30 min by the majority of electrodes (figure 2(F)). Our findings indicate that the INV-MPS can continuously monitor activity generated in 3D nerve terminals, providing a valuable tool for studying the mechanisms involved in peripheral inflammatory pain. Examining electrode response rates following capsaicin application, we found that a response rate of over 80% can be achieved within 6 d from plating. This is longer compared to typical MEA recordings of DRG cultures in 2D (2–3 d), most likely due to the additional time required for neurites to extend into the axonal compartment (figures 2(G) and (H)). Application of different doses of capsaicin (0.1–1.0 μM) on day 6 revealed a direct relationship between the concentration of the agonist and the number of observed responses and their potency (figures 2(I) and (J)), suggesting that the INV-MPS could facilitate applications in drug discovery. In summary, the INV-MPS could be utilized to study the engagement of specific ligand-gated receptors or voltage-gated ion channels that may play a role in modulating pain states, as well as to monitor the potential of various factors to induce neuronal outgrowth or nerve degeneration in toxicity studies.

2.3. Induction of sensory neurite outgrowth by colorectal cancer spheroids in the absence of NGF supplementation

We then examined whether the INV-MPS could be utilized as a tool for evaluating changes in nerve density and innervation induced by cancer in a neuron-cancer coculture. This investigation could contribute to the comprehension of the underlying neuronal mechanisms involved in pathological pain *in vivo* [25–28]. We seeded DRG neurons in the somatic compartments of the SLE INV-MPS, while colorectal (HT29) or pancreatic (PANC1) cancer spheroids were seeded in the axonal compartment. HT29 spheroids compacted efficiently and exhibited a round morphology (between 50–75 μm in diameter), whereas PANC1 spheroids tended to have a less homogeneous morphology and were larger (between 100–150 μm), as shown in figures 3(A) and (C). We monitored neurites as they traversed the barrier and innervated axonal targets following application of NGF to the distal compartment (NGF −/+). No cancer-mediated effects on neuronal outgrowth were observed compared to the NGF −/+ control condition (figures 3(A) and (B)). This suggests that NGF in the media of the axonal compartment may saturate the outgrowth potential of nerve fibers and override guidance clues. Therefore, we opted to omit NGF from the cocultures (NGF −/−) and were then able to demonstrate a cancer-mediated increase in nerve fiber density in the axonal compartment of HT29—DRG cocultures (figures 3(C) and (D)). Remarkably, we were able to simultaneously demonstrate innervation and complete envelopment of individual cancer spheroids, as observed *in vivo* [16, 19]. 3D representations of nerve fibers extending into the axonal compartments among resident cancer spheroids further confirm that the described cell-cell interactions occur in all dimensions (figures 3(E) and (F) and movies S4, S5, S6 and S7). Furthermore, for optimal comparison of neuronal outgrowth conditions and standardization, cancer cells were cultivated in neuronal media instead of cancer media without clear negative effects on viability of the cancer spheroids (SI appendix, figures S3(A) and (B)). Interestingly, while HT29—DRG cocultures exhibited a significant enhancement of neuronal outgrowth compared to control conditions (DRG alone, NGF −/−), this effect was not observed in PANC1—DRG cocultures (figures 3(C) and (D)). This observation suggests that innervation can be highly cell-type-specific, possibly due to the presence of different molecular or paracrine cues associated to the microenvironment of each cancer type.

2.4. Sensory neurons innervating 3D colorectal cancer spheroids can be activated by pain mediators

The combination of electrical and image-based techniques is crucial for investigating neuronal functions. However, current methods for monitoring activity in 3D tissues, such as calcium imaging, are typically limited to qualitative analysis. In this study, we demonstrate the potential of the MEA-integrated INV-MPS for screening purposes in pain research. As shown in figure 3, cancer spheroids occupying the axonal compartment of the SLE INV-MPS can stimulate nerve growth, raising the question of whether nerve terminals also exhibit excitability (Movie S8). To address this, we applied either capsaicin or bradykinin to the axonal compartment of INV-MPSs containing DRG (NGF−/−). with or without cancer spheroids. Prior to chemical excitation, we confirmed that HT29 did not cause any rise in spontaneous activity (SI appendix, figure S4(A)). In the presence of cancer spheroids it was possible to measure characteristic responses to both compounds in axonally extended nerve fibers, which were absent in the control group (figures 4(A) and (B)). Although the responses were less pronounced than those evoked in DRG monocultures (NGF−/+; figures 2(E)–(J)), our data suggests that the inclusion of HT29 cancer spheroids not only drives neurite outgrowth, but it is sufficient to induce nerve terminal excitation in

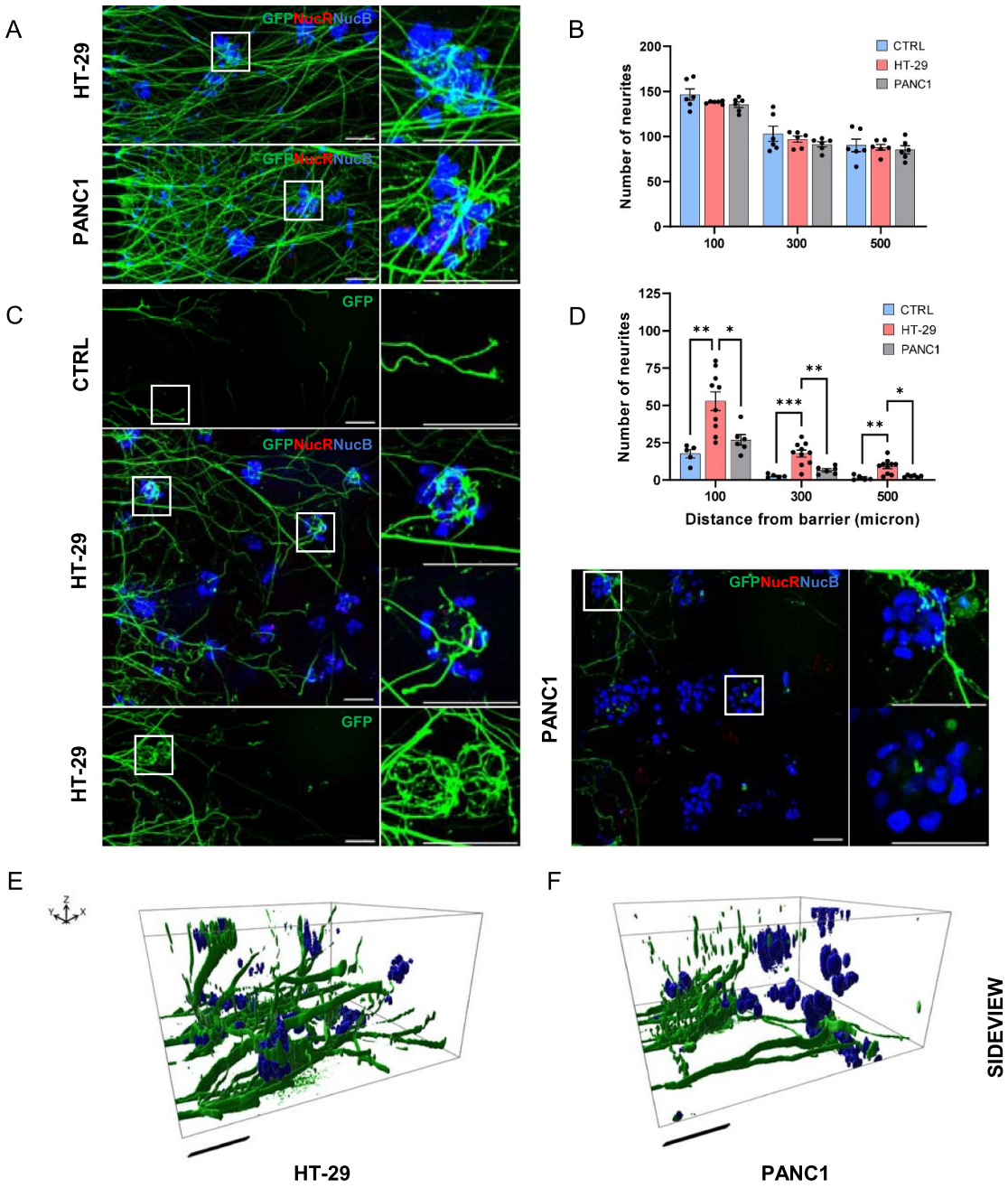

Figure 3. Induction of sensory neurite outgrowth by colorectal cancer spheroids in the absence of NGF supplementation. (A) Live-cell confocal images of GFP-transduced DRG neurons protruding from the micro tunnel-barrier and innervating either HT29 (colorectal) or PANC1 (pancreatic) cancer spheroids in 3D after 6 d in a NGF −/+ culture. Cancer spheroids are visualized using dyes staining nuclei (NucB) and dead cells (NucR). (Scale bar: 75 μm). (B) Quantification of neurite outgrowth after 6 d in culture. CTRL represents a DRG-only (NGF −/+) culture at day 5 & 6. Bar graphs represent mean ± SEM ($n = 6$ wells). (C) Live-cell confocal images of DRG neurons protruding from the micro tunnel-barrier and innervating either HT29 or PANC1 cancer spheroids after 6 d in a NGF −/− culture. (D) Quantification of neurite outgrowth after 6 d in culture. CTRL represents a DRG-only (NGF −/−) culture ($n = 5$–10 wells). (E) Sideview of 3D-surface renderings of sensory neurites innervating HT29 or (F) PANC1 cancer spheroids. Dimensions 400 × 400 × 200 μm. (Scale bar: 100 μm). In B and D, significant differences between mean values of groups are displayed as asterisks: $*p < 0.05$; $**p < 0.01$; $***p < 0.001$; $****p < 0.0001$; Brown–Forsythe and Welch's ANOVA test.

response to chemical stimuli. The response to both depolarizing stimuli was quantified and compared between DRG and HT29 coculture vs. DRG control (figures 4(C) and (D) and SI appendix, figure S4(B)). The results show that capsaicin application to HT29 coculture induced responses characterized by a less pronounced initial cumulative peak and lower responsiveness compared to NGF−/+ conditions (figures 2(I) and (J)), which is consistent with the difference in neurite outgrowth (<50%). Deeper analysis, including time-course and number of responses elicited by capsaicin or bradykinin applied to DRG (NGF−/−) alone or cocultured with HT29 cancer spheroids, revealed that colorectal cells

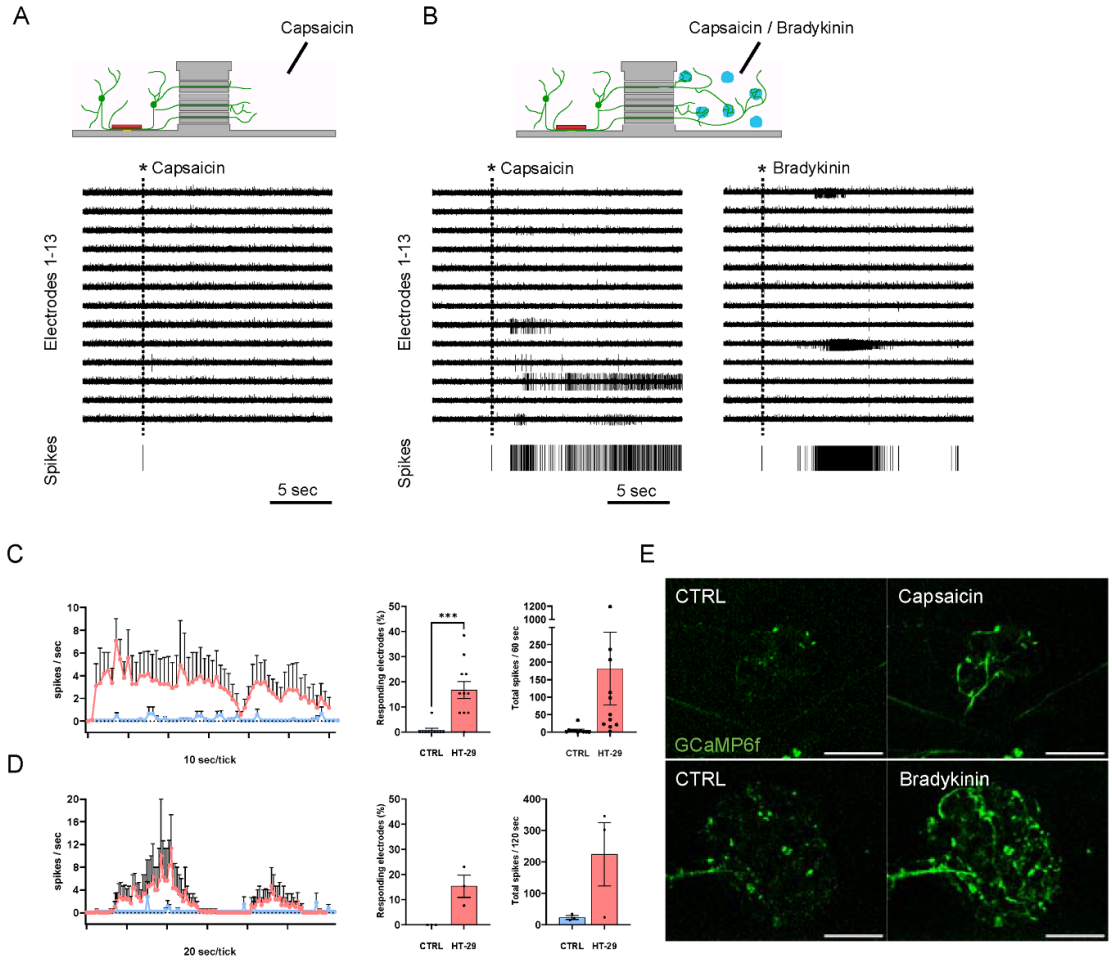

Figure 4. Sensory neurons innervating 3D colorectal cancer spheroids can be activated by pain mediators. (A) Trace plots representing individual CMEs (1–13) and cumulative raster after application of 1.0 μM Capsaicin (black asterisk) to a DRG-only culture (NGF −/−) after 6 d. (B) Trace plots and cumulative raster after application of 1.0 μM Capsaicin or 1.0 μM Bradykinin to DRG neurons innervating HT29 cancer spheroids (NGF −/−) after 6 d. (C) Temporal dynamics of capsaicin responses in DRG neurons innervating HT29 cancer spheroids (NGF −/−). Dots represent the mean spikes per second per well over a 60-second span post-application ($n = 10$–11 wells). Bar graphs comparing excitability of DRG neurons responding to axonal stimuli (percentage of responding electrodes) and total spikes recorded per well in the 60-second span post application. (D) Temporal dynamics of bradykinin responses in NGF −/− cultures of DRG neurons innervating HT29 cancer spheroids. Dots represent the mean spikes per second per well over a 120-second span post-application ($n = 3$ wells). Bar graphs comparing excitability of DRG neurons responding to axonal stimuli (percentage of responding electrodes) and total spikes recorded per well in the 120-second span post application. (E) Live-cell confocal images of GCaMP6f-transduced DRG neurons innervating HT29 cancer spheroids after 6 d in a NGF −/− culture. Application of 1.0 μM Capsaicin and 4.0 μM Bradykinin induces Ca^{2+} transients (also seen in movies S9 and S10). In C and D, significant differences between mean values of groups are displayed as asterisks: $*p < 0.05$; $**p < 0.01$; $***p < 0.001$; $****p < 0.0001$; Brown–Forsythe and Welch's ANOVA test.

have the capacity to enhance both outgrowth of 3D nerve terminals and transduction of noxious stimuli into action potentials. To explore a more direct association between nerve terminal excitability and cancer innervation, we employed AAV-GCaMPf6 to directly visualize calcium transients induced by application of chemical agonists in DRG neurons innervating cancer spheroids (figure 4(E) and movies S9 and S10). Although Ca^{2+} imaging can indeed provide an optical measure of nerve terminal activation, monitoring responses in a multiplexed 3D setting remains technically challenging and time consuming, which emphasizes the advantages of the INV-MPS platform for quantifying electrical excitability in 3D microtissues.

3. Discussion

The MPS-field aims to replicate human organ functions not properly mimicked by conventional cell cultures or animal models [29]. However, MPSs for the study of organ innervation are currently not available due to the added complexity of incorporating nerve fibers, despite the potential benefits for therapeutic domains such as visceral pain, metabolic and cardiovascular disease and neurological disorders [30]. Novel designs and platforms are required to integrate peripheral neurons and target tissues, whilst providing a robust electrophysiological readout that is consistent with neuronal activity. By accurately monitoring and controlling electrical

activity of innervating fibers, these will aid the understanding of underlying mechanisms that drive peripheral neuron-tissue interaction leading to pathological phenotypes. Leveraging expertise in combining custom MEA, high-resolution laser glass etching and 3D neuronal cultures [10], we developed an innervation platform that meets the requirements of the MPS-field towards creating intricate tissue models and incorporates a reliable electrophysiological readout. Unlike conventional 2D axonal outgrowth models [31], the INV-MPS is used to closely mimic 3D *in vivo*-like nerve-tissue interplay and simultaneously overcomes the limitations of conventional MEA systems solely designed for recording from 2D cultures. This is achieved by integrating CMEs that allow electrophysiological recording from 3D peripheral nerve fibers innervating hydrogel-embedded target tissues. Distinct from alternative methods such as patch-clamp, our approach presents several unique features, including non-invasive readout, enhanced throughput, simple handling, and seamless integration across platforms. Notably, the INV-MPS avoids the utilization of patterned polymers such as PDMS, as it is susceptible to small molecule absorption and requires a time-consuming molding procedure, among other considerations. Instead, we designed an easy-to-assemble, reusable device utilizing a glass microfluidic chip and MEA to compartmentalize and record from cultured sensory neurons, effectively ensuring the required separation of soma and terminals through barrier-etched microtunnels [5]. Axonal growth through the barrier was shown to be strongly dependent on a NGF gradient across the 3D hydrogel, closely mimicking physiologically relevant nerve guidance [32]. This was further demonstrated in the NGF +/+ condition, where the externally administered large neurotrophin pool above the DRG soma serves as a primary cue for the growth of neurites in this compartment. This overrides the growth toward the axonal compartment, despite the presence also here of NGF, as neurites would need to extend through the barrier to reach this compartment. We demonstrated that our platform enables non-invasive measurement of the electrical activity of 3D sensory terminals and that the response profiles to pain mediators are similar to those observed *in vivo* and *ex vivo* [33, 34]. For instance PGE_2, a component of the IS, exerts a crucial influence on the sensitization of nociceptive terminals in the NGF −/+ condition, impacting their excitability. Notably, both *in vivo* and *in vitro* studies consistently demonstrate that PGE_2 enhances the sensitivity of nociceptive neurons [35]. Overall, these results suggest that the INV-MPS can provide a physiological relevant measure of the engagement of receptors and ion channels localized at distinct locations (terminal vs. somatic) potentially mediating nociception. Simultaneously, it allows for the monitoring of neurotrophic factors/inhibitors' effects on neuronal outgrowth and arborization, providing valuable insights into these processes. Next, we aimed to apply INV-MPS' unique readout capabilities to the study of disease-related phenotypes by exploring CIP. Our findings indicate that when cancer spheroids and DRG neurons are cocultured in the presence of NGF, neural outgrowth is primarily driven by the exogenously applied neurotrophin in the axonal compartment. Remarkably, we observed that when NGF is omitted, the presence of colorectal cancer spheroids is sufficient to stimulate neural outgrowth and ultimately the innervation of individual cancer structures, as observed *in vivo* [16, 19]. This emphasizes the complex interplay between cancer and the PNS, highlighting the need to consider the impact of exogenously applied NGF or other growth factors when studying nerves and nerve-tissue crosstalk *in vitro*. Understanding the role of released factors is crucial to elucidate underlying mechanisms of chronic pain and identify potential therapeutic targets for the management of CIP. An increase in nerve fiber density could be demonstrated for colorectal cancer spheroids (HT29) but not for pancreatic cancer spheroids (PANC1). However, it would be premature to conclude that pancreatic cancer cannot induce outgrowth within the INV-MPS setting, as induction of axonal growth can have varying degrees of dependency on tumor-associated stromal cells and inflammation [16, 36–40], only partially recapitulated here. Neuronal outgrowth was clearly shown to depend on exogenously applied NGF, suggesting a potential correlation between the observed cancer-mediated outgrowth and NGF presence. However, given that both HT29 and PANC1 release comparable amounts of NGF *in vitro* [41, 42], the observed disparity in innervation between these two cancer types poses that NGF release alone may not be sufficient to drive outgrowth in this specific *in vitro* context. Expanding on this by investigating putative paracrine mediators and exploring alterations in gene expression and regulation of relevant protein levels is beyond the scope of our current study. However, the observed difference in 3D innervation between colorectal and pancreatic cancer spheroids emphasizes the ability of the INV-MPS to accurately recapitulate and detect differences in cancer-specific environments. This was further assessed by measuring the electrophysiological response to prototypic noxious and inflammatory stimuli in innervating fibers of HT29—DRG neuron cocultures. Here, nerve terminals extending into the axonal compartment and enveloping cancer spheroids were found to respond to both capsaicin and bradykinin. Measured responses were remarkably greater (duration and frequency) than those observed in cultures without cancer and exogenously applied NGF. This was complemented by live-imaging of evoked calcium transients occurring in 3D cancer-innervating fibers, providing a direct qualitative evaluation of tumor innervation and neuronal activity. Having the ability to additionally image

nerve terminals and cancer cells in direct contact suggests that the INV-MPS holds potential as a valuable multimodal platform for investigating the reciprocal influences between cancer and closely associated innervating fibers. While the primary objective of this study was to validate the INV-MPS by examining the impact of cancer microtissues on sensory innervation and excitability, emerging evidence indicates that peripheral neurons may additionally influence cancer homeostasis and dissemination [43], making it a promising avenue for future exploration using this *in vitro* model. The potential applications of the INV-MPS extend beyond CIP and cancer, as this model offers the opportunity to investigate a diverse array of diseases by faithfully reproducing 3D peripheral innervation and measuring excitability in various tissues. In conclusion, the INV-MPS is purposefully designed to facilitate the exploration of complex *in vitro* biology, presenting great potential for researchers in the MPS field who seek to understand the intricate interactions between the PNS and innervated organs.

4. Materials and methods

4.1. Animals

Wild-type Swiss mice obtained from Janvier Labs (France) were housed in the animal facility of the institute. Mice were kept under standard conditions with controlled temperature and a 12-hour light-dark cycle, with ad libitum access to food and water. All experimental procedures described below were performed in compliance with the regulations outlined in the European Union (EU) legislation for the care and use of laboratory animals (Directive 2010/63/EU of the European Parliament on the protection of animals used for scientific purposes) and the German TierSchG (Tierschutzgesetz) with the latest revision in 2019.

4.2. Microfabrication

INV-MPS devices were prepared following the protocol described previously [10], with modifications. Briefly, compartmentalized microfluidic chips (see SI appendix, figure S1(A)) were fabricated by SLE using fused silica. MEAs with integrated CME were produced by structuring two layers of permanent epoxy photoresist on gold microelectrodes. SU-8 2002 (MicroChem, USA) was spin-coated to achieve a thickness of approximately 3.0 μm (10 s at 500 rpm, then 30 s at 1000 rpm) (see SI appendix, figure S1(B)). ADEX TDFS A20 (Micro Resist Technology GmbH, Germany) was then laminated onto the SU-8 layer using a pouch laminator (GMP Photonex@325, EF02015) at a temperature of 75 °C. Microfluidic chips were bonded to the MEA using EPO-TEK 301-2FL (Epoxy Technology) after alignment with a Fineplacer® lambda (Finetech GmbH, Germany). The bonded devices were cured at 80 °C for 3 h. Prior to use, the devices were rinsed with bi-distilled water and incubated in a 1% Tergazyme solution for 3 h. Subsequently, they were washed overnight with bi-distilled water. This cleaning process was repeated between experiments if the devices were deemed suitable for reuse. Alternatively, the devices were detached from the MEA substrate by immersion in concentrated sulfuric acid (H2SO4 ROTIPURAN® 98%—Carl Roth, # H290-H314) overnight and then reattached to a new MEA substrate. SLE INV-MPS devices do not acquire additional assembly as they are created from a monolithic fused silica substrate and lack microelectrodes.

4.3. Fused silica microfluidic chip production

Fabrication of fused silica microfluidic chips is based on a subtractive, direct-write microfabrication process. Exploiting a femtosecond laser and etching creates integrated 3D micro-systems with micrometer precision [44]. The process exploits highly localized material modifications, triggered by non-linear absorption during the laser exposure step. The size of the modified region is in the order of 2.0 μm in *XY*-axis and from 10.0 μm to 100.0 μm in *Z*-axis, depending on the optics used to focus the laser. These modifications cause a local increase of 'etching rate' in the exposed material. Since modification happens only within the focal spot (voxel) e.g., buried structures or free-form surfaces can be produced. The exposed material is later etched in KOH based solution to create 3D devices.

4.4. Profilometry

Barrier integrated microtunnels were analyzed using a 3D optical profiler (Contour GTK-A, Bruker UK Ltd) equipped white light illumination and a 10x magnification objective. The instrument provides lateral resolution of 1.0 μm and Z resolution below 10.0 nm. Stylus profilometry (DektakXT, Bruker UK Ltd) was performed to characterize CME height. Both SU8 (no ADEX cap) and SU8-ADEX (with cap) were measured by using a 2.0 μm tip. Both sets of measurements were processed and analyzed using dedicated Vision64 software (Bruker UK Ltd).

4.5. 3D DRG neuron culture

DRG neurons were isolated and dissociated by modification of a previously published protocol [45]. Postnatal mice (P4-6) were sacrificed by decapitation and a narrow incision through the skin and muscle of the back exposed the spine, after which the ganglia could be removed for preservation in Hibernate™-A Medium (Thermo Fisher, #A1247501). Cleaned ganglia were then incubated in enzymatic solution(s) containing collagenase (IV) (Worthington, #LS004186) and dispase (Worthington, #LS02109), followed by manual dissociation in DNAse solution (Worthington, #LS002139). Lastly, gradient centrifugation was

performed to remove dead cells and debris before mixing with plating media Neurobasal-A (Thermo Fisher, #10888-022) with GlutaMAX (Thermo Fisher, #35050-038), SM1 (Stemcell, #5711), N2 Supplement-A (Stemcell, #7152), 0.5% Penicillin–Streptomycin (Sigma, #P4333) and w/wo 100 ng/mL Nerve Growth Factor 2.5 S (Promega, #G5141). Cell suspension was counted using a NucleoCounter NC-200 (ChemoMetec A/S, Denmark) and mixed with Matrigel® Growth Factor Reduced (Corning, #356230) at 1:4 ratio, resulting in a complex modulus of 20 ± 2 Pa (mean ± SD), and kept in a cold rack to prevent matrigel polymerization during seeding. Up to 5 INV-MPS devices were simultaneously sterilized/hydrophilized by air plasma treatment (Piccolo, Plasma Electronic GmbH). Low retention tips were used to dispense 8.5 μl of cell solution into each proximal channel of a single compartmentalized experiment (gel layer 1000.0 μm thick—9 total), followed by similar filling of the distal channel w/wo cancer cells. DRG neurons were plated at RT with stand. conc. 800 cells μl^{-1} (3200 cells μl^{-1} before mixing) and left to polymerize before addition of 100 μl Neurobasal-A to the media layer. 3D cultures were maintained up to 1 week by adding fresh Neurobasal-A medium every day (50/50) until electrophysiological or imaging readout.

4.6. AAV1-eGFP and AAV1-GCaMP6f transduction

DRG neurons cultured in 3D were transduced immediately after plating with adeno-associated virus serotype 1 (AAV1) vectors containing either a transgene encoding eGFP or a G-protein coupled calcium indicator (GCaMP6f), both under control of the human Synapsin 1 (hSyn) promoter. Viral particles pAAV-hSynEGFP and pAAV-hSyn-GCaMP6f.WPRE.SV40, were obtained from Addgene (catalog #50465 and #100837, respectively). The multiplicity of infection used was 105. After 3–4 d in culture, DRG neurons exhibited homogeneous green fluorescence in the case of eGFP, while GCaMP6f-labeled DRG neurons showed fluorescence specifically upon Ca^{2+} transients.

4.7. Cancer spheroid culture preparation

Human colorectal adenocarcinoma (ATCC, #SK809) and human pancreatic carcinoma (ATCC, #CRL1469) cells were grown in McCoy's 5 A medium (Gibco, #16600082) and Dulbecco's Modified Eagle's medium (Gibco, #11965092), respectively, both supplemented with 10% Fetal Bovine Serum (Gibco, 10 499 044) and 1% Penicillin–Streptomycin (Sigma, #P4333). Cells were seeded onto uncoated T75 flasks at a density of 1.0 × 106 cells per flask. On plating day, cells were detached with Trypsin-EDTA 0.25% (Sigma, T4049) for 3 min at 37 °C, °enzymatic digestion was then blocked using DMEM (Gibco, 31966-021) with 10% FBS and cells were spun down before resuspending in complementary cancer media or Neurobasal-A for plating. As described in '3D DRG neuron culture', cell suspensions were similarly counted using a NucleoCounter NC-200, mixed with Matrigel 1:4 for stand. conc. of 500 cells μl^{-1} (2000 cells μl^{-1} before mixing) and kept cold while preparing INV-MPS devices. For neuron-cancer coculture experiments—after dispensing 8.5 μl of DRG solution into the proximal compartment, either HT29 or PANC1 cell solution was dispensed into the distal compartment at RT and left to polymerize to ensure optimal 3D distribution. 100 μl Neurobasal-A w/wo NGF (100 ng ml^{-1}) (or cancer media for live-dead assays) was then added on top in the media layer and cells were closely monitored throughout the week to qualify their aggregation into cancer spheroids. 3D cultures were maintained up to 1 week, by adding fresh medium every day (50/50) until electrophysiological or imaging readout.

4.8. Fluorescence imaging of neurite growth and innervation

3D structures were imaged by a spinning disk microscope (Zeiss Cell Observer®) equipped with ZEN software (blue edition, ZEISS), followed by quantitative analysis using open-source image processing software, FIJI (ImageJ, http://imagej.nih.gov/ij/) or qualitative reconstruction with IMARIS 4.6 (Bitplane AG, Oxford Instruments). A dedicated 384 well microplate adaptor was designed and produced by Weerg Srl (Italy) to simultaneously hold two devices while imaging under humidity/CO2/temperature control (SI appendix, figure 2(B)). Neurite outgrowth assays (SI appendix, figure 2(C)) were performed on maximum intensity projections of 100 slices (AAV1-eGFP Alexa Fluor 488—*z*-axis with 0,75 μm spacing—20*x*) for 3 randomly selected ROIs (700 μm × 700 μm) starting at substrate-height. For each ROI, intensity profiles of vertical lines were plotted at 100 μm, 300 μm and 500 μm distance from distal tunnel exits and a 'Find Peaks' algorithm was then applied that returns the number of maxima (representing neurites—after background subtraction) (available from https://github.com/tferr/Scripts#ij-bar/). Neuron-cancer cocultures were quantified for neuronal outgrowth by identical image generation and processing with additional pre-incubation (3 drops ml^{-1} for 90 min at 37 °C) of NucRed Dead 647 ReadyProbes™ Reagent (TO-PRO-3 iodide) (Invitrogen, #R37113) for dead cells and NucBlue Live ReadyProbes™ Reagent (Hoechst 33 342) (Thermo Fisher, #R37605) for all nuclei.

4.9. Dextran diffusion

Barrier permeability assay was performed using 2 different fluorescently labelled dextran moieties. Four kDa FITC-Dextran and 20 kDa Rhodamine–Dextran (100 μg ml^{-1} diluted in growth media) were administered and tracked simultaneously upon pipetting of 50 μl tracer solution into 50 μl bare culture media

in the media layer (2x final conc.). A 1 × 5 tilescan (350 μm × 1750 μm—center tile containing the 300 μm barrier) was taken at substrate-height every 10 min for 12 h with $T = 0$ min directly after application. Diffusion was quantified at selected timepoints by generating intensity profiles for rectangular ROIs right outside the microtunnels (somatic and axonal compartments) and in the bulk (somatic). Time-dependent tracer loss to the somatic channel was then accounted for by measuring the fluorescent intensity development in both compartments and normalized as a % of the highest value measured axonally (at $T = 12$ h).

4.10. Calcium imaging

Neuron-cancer cocultures were transduced as described in 'AAV1-eGFP and AAV1-GCaMP6f transduction'. Adeno-associated virus expressing GCaMP6f as Ca^{2+} indicator was imaged before and immediately after application of inflammatory/excitatory compounds using a spinning disk Zeiss Cell Observer® System (20x/63x objective) and processed in FIJI. At 5–6 d in culture, cocultures were placed inside the 384 well microplate adaptor and left to acclimate. ROI (350 μm × 350 μm) was selected by qualifying the presence of innervated cancer spheroids at various heights within the gel layer before stimulation with either 4 μM Bradykinin (Tocris/Biotechne, #3004) or 1 μM Capsaicin (Tocris/Biotechne, #0462). Acquisition time was set at ∼2 frames per second.

4.11. MEA-based electrophysiological recordings

Electrophysiology of 3D innervating fibers was recorded using a USB-MEA 120-System (Multi Channel Systems MCS GmbH, Germany) at 4–6 d in culture for DRG monocultures and at 6 d in culture for cancer cocultures. During experiments, a customized MEA incubation chamber (Okolab Srl, Italy) was used to continuously monitor temperature, CO2 and humidity. The temperature was set to 36 °C, humidity at 85% and CO2 at 5%. MEAs were allowed to acclimate inside the MEA chamber before applying agonists and inflammatory mediators to the axonal compartment. Agonists were applied 30 s into a recording to identify spontaneously active electrodes. Inflammatory mediators were applied 5 min before recording. Recordings were acquired using MC_Rack v. 4.6.2 (Multichannel Systems MCS GmbH, Germany) and filtered using a fourth-order bandpass filter (60–6000 Hz), before processing with NeuroExplorer (version 5.300) for spike detection and further analysis.

4.12. Statistical analysis

Statistical analysis was performed on the collected data using GraphPad Prism 8 developed by GraphPad Software Inc. (Boston, USA). Degree of normality of the data distribution was assessed both visually and quantitatively by employing quantile-quantile plots, frequency histograms, and Shapiro-Wilks tests. Within the neurite outgrowth assay domain, conditions are represented as bar graphs with mean ± SEM. Differences were assessed by Brown–Forsythe and Welch's ANOVA test with post-hoc test Dunnett $T3$ ($n < 50$) for comparison of means. Electrophysiological data were represented as either bar graphs comparing conditions or connected-points for temporal dynamics with mean ± SEM. Differences were assessed similarly by either Brown–Forsythe and Welch's ANOVA with post hoc test Dunnett $T3$ ($n < 50$) or Welch's unpaired t-tests for comparison of means. Asterisks denote statistical significance as follows: $*p < 0.05$; $**p < 0.01$; $***p < 0.001$; $****p < 0.0001$.

Data availability statement

All data that support the findings of this study are included within the article (and any supplementary information files).

Acknowledgments

We thank Rosanna Toscano (FEMTOprint, Muzzano, CH) for fruitful discussions on glass microfluidics, Anna-Lena Keller (Tumor Biology, NMI) for supplying the human cancer cell lines and Michael Mierzejewski, Peter Jones (Bio-medical Micro and Nano Engineering, NMI) and Eduardo Brás (Organ-on-Chip, NMI) for technical assistance. We also thank Frank Machnow (NMI) for comprehensive 3D modelling and Martin Kriebel (Molecular Biology & Neurobiology, NMI) for confocal microscopy assistance.

Conflict of interest

P.C. is named as inventor on patent application WO2019115320A1 ('Device for the examination of neurons') filed by NMI Natural and Medical Sciences Institute at the University of Tübingen.

Funding

P C acknowledges funding from the State Ministry of Baden-Württemberg for Economic Affairs, Labour and Housing Construction. M v d M and P C acknowledge funding from the European Union Horizon

2020 Framework Programme for Research an Innovation under the Marie Sklodowska-Curie Grant Agreement No. 814244 (BONEPAIN II). P C acknowledges funding from Eureka's Eurostars Programme under grant Agreement 115217 (NEUROCHIP). FE acknowledges funding from the Ministry of National Education of Turkey.

Research animals ethics statement

All animal research procedures were conducted in accordance with the EU legislation for the care and use of laboratory animals (Directive 2010/63/ EU) and the German Animal Welfare Act ('Tierschutzgesetz', 2019).

Author contributions

Work	MvdM	FE	SM	AL	PL	PC
Conceptualization: Experimental design						
Methodology: MEA design						
Methodology: CME microfabrication						
Methodology: Glass device production						
Methodology: Assembly						
Methodology: Cell culture						
Investigation: Neurite outgrowth						
Investigation: Diffusion assay						
Investigation: Ca^{2+} imaging and confocal microscopy						
Investigation: Electrophysiological recordings						
Formal analysis: Statistics						
Formal analysis: Electrophysiology						
Visualization: Data presentation						
Original draft						
Review and editing						
Funding acquisition						

ORCID iDs

Matthijs van der Moolen https://orcid.org/0000-0003-3999-7226
Fulya Ersoy https://orcid.org/0000-0001-7795-3019
Paolo Cesare https://orcid.org/0000-0003-1324-5974

References

[1] Park D, Lee J, Chung J J, Jung Y and Kim S H 2020 Integrating organs-on-chips: multiplexing, scaling, vascularization, and innervation *Trends Biotechnol.* **38** 99–112
[2] Rajendran P S *et al* 2019 Identification of peripheral neural circuits that regulate heart rate using optogenetic and viral vector strategies *Nat. Commun.* **10** 1944
[3] Takahashi S, Ishida A, Kubo A, Kawasaki H, Ochiai S, Nakayama M, Koseki H, Amagai M and Okada T 2019 Homeostatic pruning and activity of epidermal nerves are dysregulated in barrier-impaired skin during chronic itch development *Sci. Rep.* **9** 8625
[4] Guo X, Colon A, Akanda N, Spradling S, Stancescu M, Martin C and Hickman J J 2017 Tissue engineering the mechanosensory circuit of the stretch reflex arc with human stem cells: sensory neuron innervation of intrafusal muscle fibers *Biomaterials* **122** 179–87
[5] Vysokov N, McMahon S B and Raouf R 2019 The role of Na(V) channels in synaptic transmission after axotomy in a microfluidic culture platform *Sci. Rep.* **9** 12915
[6] Atmaramani R, Veeramachaneni S, Mogas L V, Koppikar P, Black B J, Hammack A, Pancrazio J J and Granja-Vazquez R 2021 Investigating the function of adult DRG neuron axons using an *in vitro* microfluidic culture system *Micromachines* **12** 1317
[7] Enright H A *et al* 2016 Long-term non-invasive interrogation of human dorsal root ganglion neuronal cultures on an integrated microfluidic multielectrode array platform *Analyst* **141** 5346–57
[8] Klusch A, Gorzelanny C, Reeh P W, Schmelz M, Petersen M and Sauer S K 2018 Local NGF and GDNF levels modulate morphology and function of porcine DRG neurites, *in vitro* *PLoS One* **13** e0203215
[9] Clark A J, Menendez G, AlQatari M, Patel N, Arstad E, Schiavo G and Koltzenburg M 2018 Functional imaging in

microfluidic chambers reveals sensory neuron sensitivity is differentially regulated between neuronal regions *Pain* **159** 1413–25
[10] Molina-Martinez B, Jentsch L-V, Ersoy F, van der Moolen M, Donato S, Ness T V, Heutink P, Jones P D and Cesare P 2022 A multimodal 3D neuro-microphysiological system with neurite-trapping microelectrodes *Biofabrication* **14** 025004
[11] Neto E *et al* 2022 Osteoclast-derived extracellular vesicles are implicated in sensory neurons sprouting through the activation of epidermal growth factor signaling *Cell Biosci.* **12** 127
[12] Steins H *et al* 2022 A flexible protruding microelectrode array for neural interfacing in bioelectronic medicine *Microsyst. Nanoeng.* **8** 131
[13] Ao Z, Cai H, Wu Z, Krzesniak J, Tian C, Lai Y Y, Mackie K and Guo F 2022 Human spinal organoid-on-a-chip to model nociceptive circuitry for pain therapeutics discovery *Anal. Chem.* **94** 1365–72
[14] Guichard A, Remoué N and Honegger T 2022 *In vitro* sensitive skin models: review of the standard methods and introduction to a new disruptive technology *Cosmetics* **9** 67
[15] Mantyh P W 2019 Mechanisms that drive bone pain across the lifespan *Br. J. Clin. Pharmacol.* **85** 1103–13
[16] Jimenez-Andrade J M, Bloom A P, Stake J I, Mantyh W G, Taylor R N, Freeman K T, Ghilardi J R, Kuskowski M A and Mantyh P W 2010 Pathological sprouting of adult nociceptors in chronic prostate cancer-induced bone pain *J. Neurosci.* **30** 14649–56
[17] Gysler S M and Drapkin R 2021 Tumor innervation: peripheral nerves take control of the tumor microenvironment *J. Clin. Invest.* **131** e147276
[18] Zheng Q, Fang D, Cai J, Wan Y, Han J-S and Xing G-G 2012 Enhanced excitability of small dorsal root ganglion neurons in rats with bone cancer pain *Mol. Pain* **8** 24
[19] Bloom A P, Jimenez-Andrade J M, Taylor R N, Castañeda-Corral G, Kaczmarska M J, Freeman K T, Coughlin K A, Ghilardi J R, Kuskowski M A and Mantyh P W 2011 Breast cancer-induced bone remodeling, skeletal pain, and sprouting of sensory nerve fibers *J. Pain* **12** 698–711
[20] Haroun R, Wood J N and Sikandar S 2022 Mechanisms of cancer pain *Front. Pain Res.* **3** 1030899
[21] Zhu Y F *et al* 2016 Differences in electrophysiological properties of functionally identified nociceptive sensory neurons in an animal model of cancer-induced bone pain *Mol. Pain* **12** 1744806916628778
[22] Huang E J and Reichardt L F 2001 Neurotrophins: roles in neuronal development and function *Annu. Rev. Neurosci.* **24** 677–736
[23] Price T J, Louria M D, Candelario-Soto D, Dussor G O, Jeske N A, Patwardhan A M, Diogenes A, Trott A A, Hargreaves K M and Flores C M 2005 Treatment of trigeminal ganglion neurons *in vitro* with NGF, GDNF or BDNF: effects on neuronal survival, neurochemical properties and TRPV1-mediated neuropeptide secretion *BMC Neurosci.* **6** 4
[24] Cao E, Liao M, Cheng Y and Julius D 2013 TRPV1 structures in distinct conformations reveal activation mechanisms *Nature* **504** 113–8
[25] Albo D, Akay C L, Marshall C L, Wilks J A, Verstovsek G, Liu H, Agarwal N, Berger D H and Ayala G E 2011 Neurogenesis in colorectal cancer is a marker of aggressive tumor behavior and poor outcomes *Cancer* **117** 4834–45
[26] Gasparini G, Pellegatta M, Crippa S, Schiavo Lena M, Belfiori G, Doglioni C, Taveggia C and Falconi M 2019 Nerves and pancreatic cancer: new insights into a dangerous relationship *Cancers* **11** 893
[27] Horn A, Dahl O and Morild I 1991 Venous and neural invasion as predictors of recurrence in rectal adenocarcinoma *Dis. Colon Rectum* **34** 798–804
[28] Stopczynski R E, Normolle D P, Hartman D J, Ying H, DeBerry J J, Bielefeldt K, Rhim A D, DePinho R A, Albers K M and Davis B M 2014 Neuroplastic changes occur early in the development of pancreatic ductal adenocarcinoma *Cancer Res.* **74** 1718–27
[29] Huh D, Matthews B D, Mammoto A, Montoya-Zavala M, Hsin H Y and Ingber D E 2010 Reconstituting organ-level lung functions on a chip *Science* **328** 1662–8
[30] Das S, Gordián-Vélez W J, Ledebur H C, Mourkioti F, Rompolas P, Chen H I, Serruya M D and Cullen D K 2020 Innervation: the missing link for biofabricated tissues and organs *npj Regen. Med.* **5** 11
[31] Campenot R B 1977 Local control of neurite development by nerve growth factor *Proc. Natl Acad. Sci.* **74** 4516–9
[32] Davies A M 1988 The emerging generality of neurotrophic hypothesis *Trends Neurosci.* **11** 243–4
[33] Shu X-Q, Llinas A and Mendell L M 1999 Effects of trkB and trkC neurotrophin receptor agonists on thermal nociception a behavioral and electrophysiological study *Pain* **80** 463–70
[34] Davis K D, Meyer R A and Campbell J N 1993 Chemosensitivity and sensitization of nociceptive afferents that innervate the hairy skin of monkey *J. Neurophysiol.* **69** 1071–81
[35] Kimourtzis G, Rangwani N, Jenkins B J, McNaughton P A and Raouf R 2022 A microfluidic-based model of nociceptor sensitization reveals a direct activation of sensory axons by prostaglandin E2 *Biorxv* (https://doi.org/10.1101/2022.03.18.484883)
[36] Li X, Peng X, Yang S, Wei S, Fan Q, Liu J, Yang L and Li H 2022 Targeting tumor innervation: premises, promises, and challenges *Cell Death Discov.* **8** 131
[37] Chu X *et al* 2022 Blocking cancer-nerve crosstalk for treatment of metastatic bone cancer pain *Adv. Mater.* **34** e2108653
[38] Silverman D A, Martinez V K, Dougherty P M, Myers J N, Calin G A and Amit M 2021 Cancer-associated neurogenesis and nerve-cancer cross-talk *Cancer Res.* **81** 1431–40
[39] Gil Z, Cavel O, Kelly K, Brader P, Rein A, Gao S P, Carlson D L, Shah J P, Fong Y and Wong R J 2010 Paracrine regulation of pancreatic cancer cell invasion by peripheral nerves *J. Natl Cancer Inst.* **102** 107–18
[40] Demir I E, Friess H and Ceyhan G O 2015 Neural plasticity in pancreatitis and pancreatic cancer *Nat. Rev. Gastroenterol. Hepatol.* **12** 649–59
[41] de Farias C B, Stertz L, Lima R C, Kapczinski F, Schwartsmann G and Roesler R 2009 Reduced NGF secretion by HT-29 human colon cancer cells treated with a GRPR antagonist *Protein Pept. Lett.* **16** 650–2
[42] Zhu Z W, Friess H, Wang L, Bogardus T, Korc M, Kleeff J and Büchler M W 2001 Nerve growth factor exerts differential effects on the growth of human pancreatic cancer cells *Clin. Cancer Res.* **7** 105–12 (available at: https://pubmed.ncbi.nlm.nih.gov/11205897/)
[43] Wang H, Zheng Q, Lu Z, Wang L, Ding L, Xia L, Zhang H, Wang M, Chen Y and Li G 2021 Role of the nervous system in cancers: a review *Cell Death Discov.* **7** 76
[44] Bellouard Y 2012 The femtoprint project *J. Laser Micro/Nanoeng.* **7** 1–10
[45] Sleigh J N, Weir G A and Schiavo G 2016 A simple, step-by-step dissection protocol for the rapid isolation of mouse dorsal root ganglia *BMC Res. Notes* **9** 82